ChemPubSoc Europe

DOI: 10.1002/open.201900126

Open Access ChemistryOPEN Full Papers

Mannose-Modified Multi-Walled Carbon Nanotubes as a Delivery Nanovector Optimizing the Antigen Presentation of Dendritic Cells

Zhipeng Dong,[a] Qiyan Wang,[a] Ming Huo,[a] Nanxia Zhang,[a] Bingxia Li,[a] Hongmei Li,[a] Yisong Xu,[a] Meng Chen,[b] Hao Hong,*[c] and Yue Wang*[a]

Dendritic cells (DCs) based cancer immunotherapy is largely dependent on adequate antigen delivery and efficient induction of DCs maturation to produce sufficient antigen presentation and ultimately lead to substantial activation of tumor-specific $CD8^+$ T cells. Carbon nanotubes (CNTs) have attracted great attention in biomedicine because of their unique physicochemical properties. In order to effectively deliver tumor antigens to DCs and trigger a strong anti-tumor immune response, herein, a specific DCs target delivery system was assembled by using multi-walled carbon nanotubes modified with mannose which can specifically bind to the mannose receptor on DCs membrane. Ovalbumin (OVA) as a model antigen, could be adsorbed on the surface of mannose modified multi-walled carbon nanotubes (Man-MWCNTs) with a large drug loading content. This nanotube-antigen complex showed low cytotoxicity to DCs and was efficiently engulfed by DCs to induce DCs maturation and cytokine release in vitro, indicating that it could be a potent antigen-adjuvant nanovector of efficient antigen delivery for therapeutic purpose.

Introduction

Cancer immunotherapy represents the most novel exciting therapeutic modality for treating cancer.[1] Aiming at promoting specific and long-lasting immunity against cancer through stimulating the patients' inherent immune system to recognize and eliminate tumor cells, cancer immunotherapy is now considered as an ideal therapeutic strategy against various types of cancer.[2–4] T cells, especially cytotoxic $CD8^+$ T cells which can directly kill target tumor cells and acquire a long-lasting memory phenotype responding to cancer recurrence, play a vital role in antitumor immune response.[5] Hence, how to efficiently generate enough robust cytotoxic $CD8^+$ T cells is the main challenge of this strategy.

Known as the most professional and important antigen presenting cells (APCs), dendritic cells (DCs) are critical in initiating adaptive immune responses through activating naive T cells.[6] After capturing tumor antigen, DCs will present them in the form of a major histocompatibility complex (MHC)/peptide complex on their surface and finally elicit effective activation of both $CD8^+$ and $CD4^+$ T lymphocytes.[7] Therefore, enough tumor antigen presentation by DCs is critical in initiating antitumor immune response. Previous studies have shown that most tumors can evade recognition by the immune system via expressing low levels of antigenic epitopes, MHC, and co-stimulatory molecules, making them become poorly immunogenic to DCs.[8] In this regard, sufficient delivery of tumor antigen to DCs, which can efficiently induce DCs maturation and cross-presentation, is the key strategy of cancer immunotherapy.

Upon contact with antigens like pathogens or tumor cells, DCs can recognize and internalize them via several mechanisms. The phagocytosis of pathogens mediated by pattern recognition receptors (PRRs) such as Toll-like receptors (TLRs), NOD-like receptors (NLRs), C-type lectin receptors (CLRs) and others are crucial for the induction of proper DC maturation.[9] Among them, through carbohydrate recognition domains (CRDs) in their extracellular carboxy-terminal domains, CLRs could bind sugar moieties on the surface of certain pathogens in a calcium-dependent manner, lead to pathogen internalization via receptor mediated endocytosis and subsequent degradation, and finally present the pathogen as antigen to T cells in the context of MHC I or MHC II, or both.[10] As a member of C-type lectin receptors predominantly expressed by DCs, mannose receptor (MR) can recycle continuously between the plasma membrane and endosomal compartments in a clathrin-dependent manner, leading to more effective internalization and surface presentation of antigens by immature DCs and finally resulting in enhanced T cell activation.[11–12] Thus,

[a] Z. Dong, Q. Wang, M. Huo, N. Zhang, B. Li, H. Li, Y. Xu, Prof. Y. Wang
Key Laboratory of Biomedical Functional Materials, School of Sciences, China Pharmaceutical University, Nanjing 211198, Jiangsu Province, China
E-mail: zwy_1115@126.com
[b] M. Chen
Nanjing Foreign Language School, NO.30 East Beijing Road, Nanjing, 210029, China
[c] Prof. H. Hong
Center for Molecular Imaging, Department of Radiology, University of Michigan, Ann Arbor, Michigan 48109-2200, United States
E-mail: hahong@med.umich.edu

Supporting information for this article is available on the WWW under https://doi.org/10.1002/open.201900126

targeting to MR could be a powerful strategy to induce antigen-specific immune response.

In the past few decades, a variety of nanoparticles (NPs) based drug delivery systems have been developed for their superior properties of enhancing therapeutic outcomes such as improving loading drug's safety, prolonging circulation time and promoting bioavailability.[13–15] Carbon nanotubes (CNTs), as a type of nanomaterial with unique physical and chemical properties, have attracted a lot of interest in biomedical applications.[16] Their intrinsic properties make them convenient to internalize into a wide variety of cell types. Simultaneously, they have a large available surface area for chemical modification. Furthermore, extremely high surface area to volume ratio of CNTs can provide multiple attachment sites for various bioactive molecules such as proteins,[17] nucleic acids[18] and free drugs,[19] along with protecting them against enzymatic degradation, thus resulting in a superior intracellular biostability. Besides, their remarkable conductive properties making them have boosting effect on conductive tissue such as neural tissues.[20–22] All of these fantastic properties make CNTs available as a kind of candidate vehicle to be used in vaccine development. The preparation of carbon nanotube derivatives is usually carried out by introducing a carboxyl group by oxidation, followed by modification of other molecules. Another classical approach is to directly bind surfactants, nucleic acids, peptides, polymers or oligomers in a non-covalent manner.[23–24] Recently, there have also been reports on the use of carbon nanotubes for the delivery of antigens, but most of them just modified simply to increase their water solubility, which makes them less effective in antigen delivery.[25–27]

In this study, we developed multi-walled carbon nanotubes (MWCNTs) modified with mannose (Man-MWCNTs) as a specific target delivery system to DCs. Compared with passive target delivery, decorating with targeting ligands which can actively recognize specific receptors on the target cell is much more efficient.[28] Chicken egg ovalbumin (OVA), a standard antigenic protein,[29] was chosen and loaded onto Man-MWCNTs. (Scheme 1) It was found that this system could be highly engulfed by DCs and efficiently induce DCs maturation in vitro, demonstrating its potential as an antigen-adjuvant nanovector for further application in vaccine development.

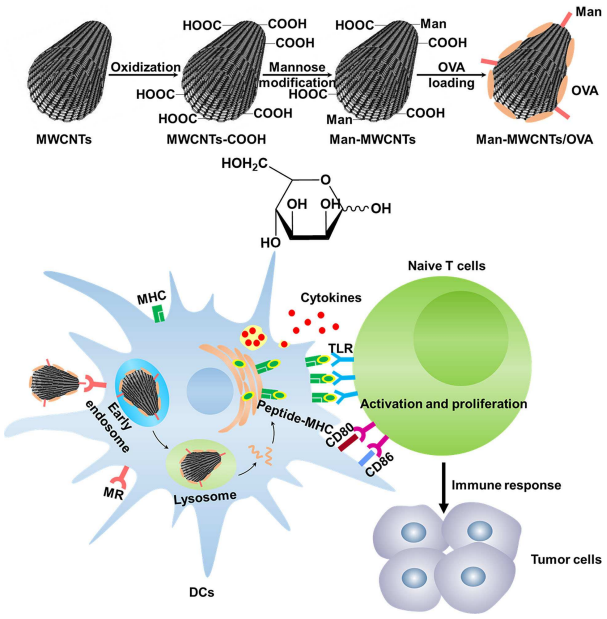

Scheme 1. Schematic illustration of Man-MWCNTs as an antigen delivery nanovector to DCs.

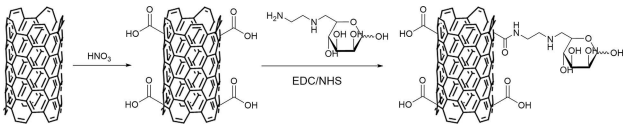

Figure 1. Synthesis of Man-MWCNTs.

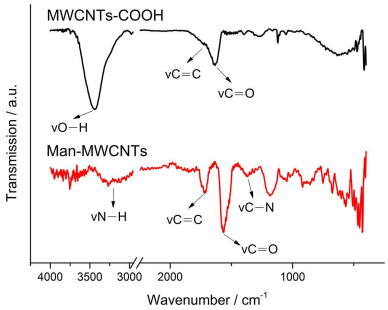

Figure 2. Infrared spectra of MWCNTs-COOH and Man-MWCNTs.

Results and Discussion

Preparation and Characterization of Man-MWCNTs/OVA

Man-MWCNTs were prepared from the oxidation of MWCNTs followed by modification with mannosylated ethylenediamine. (Figure 1) Fourier-transform infrared spectroscopy (FT-IR) spectra were recorded using a pressed disk of powder combined with KBr. As shown in Figure 2, the stretching vibration peaks of O–H at 3500 cm^{-1} and C=O at 1630 cm^{-1} showed the existence of carboxyl. After modification with mannosylated ethylenediamine, the peak at 3500 cm^{-1} decreased and the stretching vibration peak of N–H and C–N appeared at 3200 cm^{-1} and 1365 cm^{-1}, intimating the carboxyl was converted to anamide after functionalization. These results were also verified by thermogravimetric analysis (Figure 3) and are consistent with similar literature.[30] MWCNTs showed almost no significant weight loss in low temperature, while MWCNTs-COOH showed one weight loss platform (from 30 °C to 140 °C, 5.395 %) which is due to carboxyl groups. In the curve of Man-MWCNTs, the weight loss is similar to MWCNTs-COOH but slightly increased (from 30 °C to 180 °C, 6.572 %), indicating that some of the carboxyl groups have been amidated by mannosylated ethylenediamine.

Elemental analysis determined the contents of C, H and N elements in Man-MWCNTs were 75.62 wt %, 1.33 wt % and 1.86 wt %, respectively. XPS was further performed to analyze

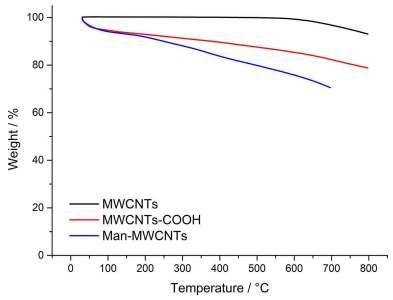

Figure 3. Thermogravimetric profiles of MWCNTs, MWCNTs-COOH and Man-MWCNTs.

the chemical compositions of the uppermost surface of the nanotubes. As shown in Figure 4a, the main peaks of C1s and O1s photoelectrons can be observed in the scanning spectra of MWCNTs-COOH and Man-MWCNTs. Deconvolution of high-resolution XPS spectra over the C1s region for all samples was conducted, as shown in Figure 4b and 4c. The C1s spectra have each been resolved into at five individual component peaks that represent carbon in graphite at 284.5 eV, carbon in aliphatic structures at 285.4 eV, carbon in phenolic, alcohol, ether at 286.8 eV, carbon in carboxyl, lactone, or ester groups at 288.7 eV, and satellite peaks due to π-π* transitions in aromatic rings at 291.2 eV (π-π* transition). The deconvolution of XPS

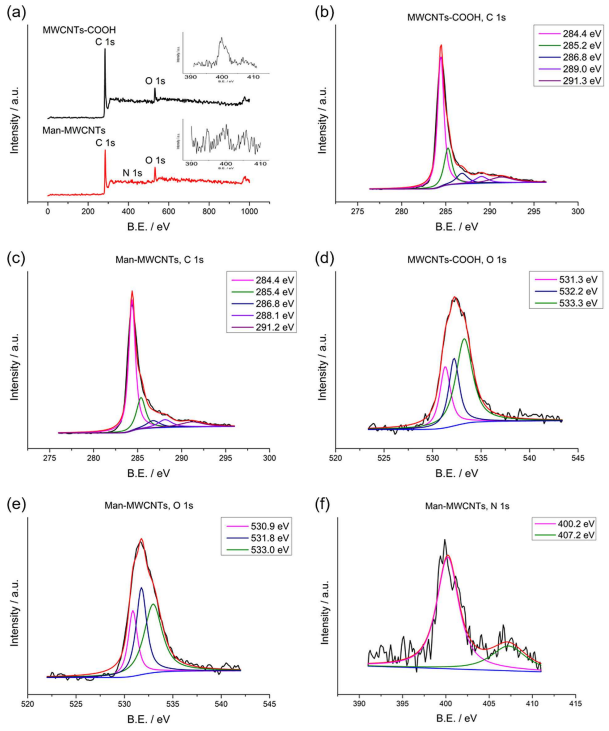

Figure 4. Results of XPS analysis of the MWCNTs-COOH and Man-MWCNTs: (a) XPS survey scan spectra of MWCNTs-COOH and Man-MWCNTs. The inset is magnification of the N1s region in MWCNTs-COOH and Man-MWCNTs spectrum. (b,c) High resolution fitted XPS C1s spectra of MWCNTs-COOH and Man-MWCNTs. (d,e) High resolution fitted XPS O1s spectra of MWCNTs-COOH and Man-MWCNTs. (f) High resolution fitted XPS N1s spectra of Man-MWCNTs.

O1s peaks gives additional information on the nature of the surface oxygen-containing groups. Figure 4d and 4e show the O1s spectrum of all samples, which can be deconvoluted into the following bands: carbonyl oxygen atoms at 531.1 eV, carbonyl oxygen atoms in carboxyls and amides at 532.4 eV and oxygen atoms in hydroxyls or ethers at 533.3 eV.[31] In addition, the slight peak of N1s photoelectrons can be observed in the spectrum of Man-MWCNTs, while in the corresponding area of MWCNTs-COOH nothing appears except noise signals (Figure 4a). The spectra of N1s in Man-MWCNTs could be deconvoluted into two bands, amide at 400.2 eV and amine at 407.2 eV (Figure 4f), which is also the evidence of the successful amidation of carboxyl groups by mannosylated ethylenediamine.[32]

OVA was then chosen as a model antigen to couple to NTs for testifying its efficiency. The successful loading of OVA on nanotubes was observed by TEM (Figure 5). The exposed

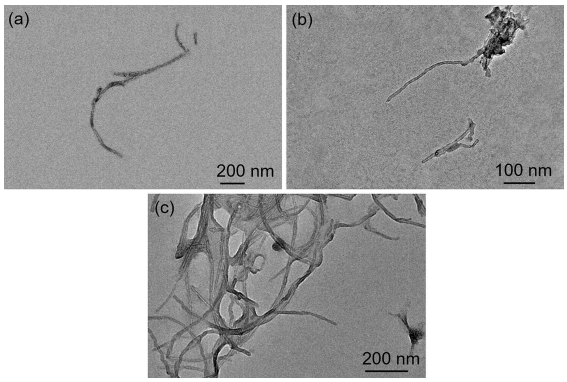

Figure 5. TEM images of (a) MWCNTs, (b) Man-MWCNTs and (c) Man-MWCNTs/OVA

nanotubular morphology of Man-MWCNTs was clearly shown in Figure 5b, which has no obvious difference from MWCNTs (Figure 5a). While after interacting with OVA, Man-MWCNTs surface was finally coated with protein layers (Figure 5c). The calculation showed that the drug loading efficiency is approximately 22.8%, indicating that much higher amount of protein could be loaded on the nanotubes' surface compared with others nanovectors.[33–35] The drug release profile showed that the Man-MWCNTs could prolong the release time of OVA and reached a cumulative release of approximately 35% at 72 h, which would help to produce long-lasting anti-tumor immune response (Figure S1).

The change of zeta potential also demonstrated the successful modification and protein covering of MWCNTs. Surface charge is typically quantified by the zeta potential, a parameter that provides information on the net charge of particles in a liquid environment. Its value is closely related to suspension stability and particle surface coating.[36] As shown in Figure 6, the zeta potential of original MWCNTs was about −21 mV. After oxidation, the potential has changed to −42 mV, which supported the above FT-IR result that there was a large amount of carboxyl groups on the surface of the nanotubes.

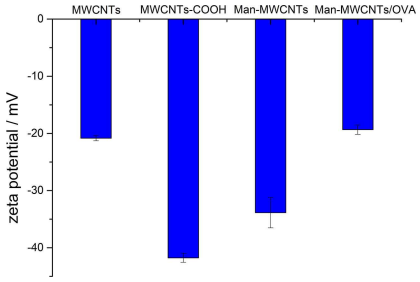

Figure 6. Zeta potentials of MWCNTs, MWCNTs-COOH, Man-MWCNTs and Man-MWCNTs/OVA.

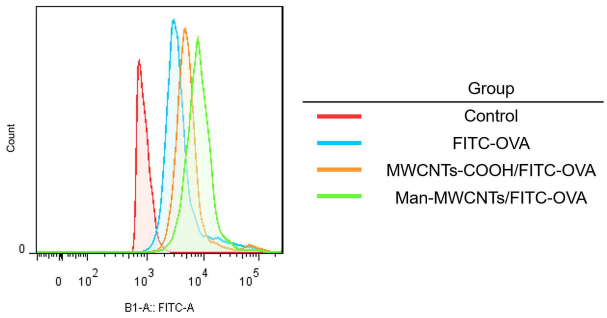

Figure 8. Flow cytometric analysis of FITC-labeled OVA in BMDCs incubated with OVA, MWCNTs-COOH/OVA, and Man-MWCNTs/OVA for 4 h.

The potential increased to −34 mV after modification of mannose, indicating that some of the carboxyl have been esterified with mannose. Furthermore, when the surface of Man-MWCNTs was covered by OVA, the zeta potential of Man-MWCNTs/OVA increased to −20 mV.

In Vitro Cytotoxicity Research

To study the potential cytotoxicity of nanotubes, BMDCs were treated with various concentrations of Man-MWCNTs and Man-MWCNTs/OVA for 12 hours. The corresponding concentrations of OVA were also tested under the same conditions in order to eliminate its interference. As shown in Figure 7a, OVA showed no significant toxicity to BMDCs at all concentrations. Figure 7b showed that in both tests, with 100 μg/mL of nanotubes, more than 60% of cells remained viable after incubation, which indicated that those nanotubes did not exert significant cytotoxicity on BMDCs. It is desirable that the loading of OVA slightly reduced the toxicity of carbon nanotubes.

Mannose-Modification Promoted Antigen Uptake in BMDCs

In order to investigate whether the modification of mannose could enhance the uptake of MWCNTs, OVA was prelabeled by FITC and used to form the MWCNTs/OVA complex, which was then incubated with BMDCs. The flow cytometric analysis in Figure 8 showed that the OVA uptake by BMDCs was significantly enhanced when OVA was loaded on MWCNTs, which is due to the ability of carbon nanotubes to internalize into cells through passive mechanisms like endocytic or needlelike penetration.[37] Moreover, uptake of OVA by mannose-modified MWCNTs increased more than unmodified ones, suggesting that modification of the target molecular-mannose could extremely enhance the binding of NTs and DCs through ligand/receptor interactions of mannose. The similar results were also revealed in confocal fluorescent microscope images (Figure 9). Higher intracellular green fluorescent intensity could be observed in cells treated with MWCNTs-COOH/OVA than OVA owing to the convenient internalization of MWCNTs, while the strongest FITC fluorescence intensity also appeared in the mannose-modified group. Furthermore, we could observe that some of the FITC labeled proteins and nanotubes were in the same position, which confirms that the proteins were indeed coated on the surface of the nanotubes and could be released after being endocytosed by BMDCs. Moreover, the green fluorescence (OVA) and red fluorescence (endosomes or lysosomes) do not completely coincide in cells treated with Man-MWCNTs/OVA, indicating that the nanotubes may help antigens escape from endosomes to cytoplasm, which is essential for exogenous antigens to be loaded onto MHC Class I molecules and finally induce $CD8^+$ cell response.[38] All these

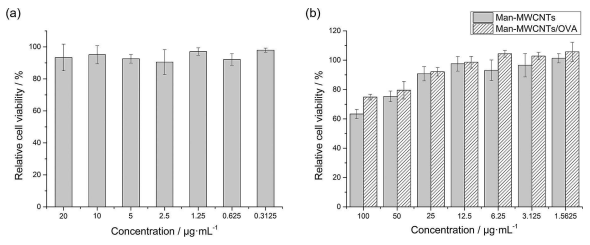

Figure 7. Cytotoxicity of (a) OVA, (b) Man-MWCNTs and Man-MWCNTs/OVA internalized by BMDCs.

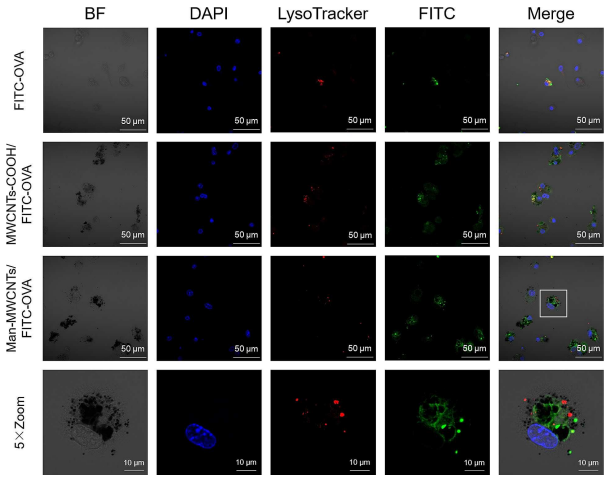

Figure 9. Confocal images of BMDCs incubated with FITC-labeled OVA, MWCNTs-COOH/FITC-OVA, and Man-MWCNTs/FITC-OVA for 4 h. Later endosomes and lysosomes (red) were stained with lysoTacker-Red, while OVA (green) were prelabeled with FITC. Nuclei (blue) were stained with DAPI.

results demonstrated that compared with OVA and MWCNTs-COOH/OVA, Man-MWCNTs/OVA could significantly increase antigen uptake of BMDCs via active surface binding.

Man-MWCNTs/OVA Induced BMDCs Maturation

In view of the fact that Man-MWCNTs has good biocompatibility and can effectively increase antigen uptake of BMDCs by target delivery, we investigated its antigen presenting effect on BMDCs in vitro. Immature DCs are powerful antigen-capturing cells, while mature DCs mainly act as antigen-presenting cells. After capturing pathogens or tumor cells, immature DCs will become mature DCs in the progress of migration from the periphery to draining lymph nodes and then present antigens through MHC complex to naive T lymphocytes, and finally initiate subsequent immune responses.[39] Thus, the level of DCs maturation is a quite important index to evaluate the immune response in DC-based immunotherapy.

DC maturation is associated with a wide range of cellular changes, one of them is the upregulation of co-stimulatory molecules (CD80, CD86) on DCs membrane.[40] Figure 10

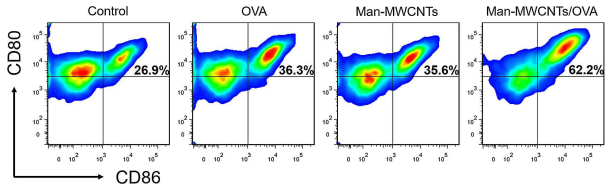

Figure 10. Quantification of $CD80^+$ and $CD86^+$ expression, which are markers for DC maturation on the surface of BMDCs ($CD11c^+$) after in vitro incubation with OVA, Man-MWCNTs, or Man-MWCNTs/OVA for 12 h by flow cytometry.

showed that in our experiments, the percent of matured DCs ($CD11c^+CD80^+CD86^+$) significantly increased from 26.9% to 62.2%, while the DC maturation level of those treated by the same dose of free OVA was only increased to 36.3%, suggesting that Man-MWCNTs/OVA-stimulated BMDCs may induce much stronger immune responses owing to the increasing uptake of antigen caused by Man-MWCNTs.

During the process of antigen-presentation, antigens will promote the activation and maturation of DCs, which not only results the expression of co-stimulatory molecules, but also leads to the secretion of cytokines.[41] It has been demonstrated that interleukin 1β (IL-1β) plays a significant role in the activation of natural killer cells for efficient priming of Th1 cells and CTLs,[42] while interleukin 6 (IL-6) is convinced to stimulate the proliferation of activated B cells to secrete antibodies and promote T cell proliferation and CTL activation.[43] Tumor necrosis factor alpha (TNF-α) plays an important role in promoting the expression of T cell MHC class I antigen and enhancing the proliferation of IL-2-dependent thymocyte and T cell.[44–45] To investigate the level of these cytokines, the culture supernatants of BMDCs were harvested after various treatment and then analyzed by an enzyme-linked immunosorbent assay

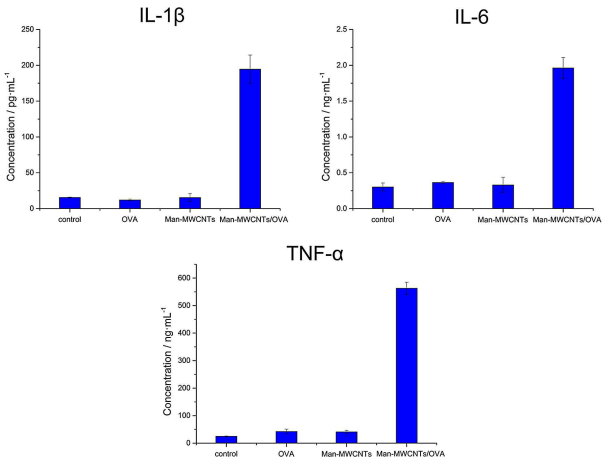

Figure 11. Secretion of IL-1β, IL-6 and TNF-α in suspensions of BMDCs after in vitro incubation with OVA, Man-MWCNTs, or Man-MWCNTs/OVA for 24 h by ELISA.

(ELISA). As shown in Figure 11, the levels of IL-1β, IL-6 and TNF-α secreted by BMDCs significantly increased after Man-MWCNTs/OVA treatment. Our results taken together suggest that Man-MWCNTs could effectively help OVA promote DC maturation and cytokine secretion to trigger a stronger immune effect by increasing DC uptake.

Conclusions

Novel DCs-targeted nanovector were fabricated by modifying the surface of MWCNTs with mannose. A high drug loading content of OVA was observed owing to the large surface area of MWCNTs. The ability of this carbon nanotube as an antigen carrier to induce and enhance DCs activation by specific interactions with the mannose receptor was investigated. Cell affinity experiment showed the modification of mannose greatly enhanced OVA target delivery to DCs, followed with the efficiently enhanced DCs maturation and cytokines secretion. All of these showed that Man-MWCNTs could be considered as a promising vehicle for antigen delivery, which offers new opportunities for tumor-specific antigen loading to induce an effective immune response in vivo.

Experimental Section

Materials

All reagents and solvents were commercially available and used without additional treatment. Multi-walled Carbon Nanotubes (length, 0.5–2 μm; diameter, < 8 nm) was purchased from XFNANO (Nanjing, China). D-mannose, N-(3-dimethylaminopropyl)-N-ethyl-carbodiimide (EDC), 2-(N-morpholino) ethanesulfonic acid (MES) and fluorescein isothiocyanate (FITC) were purchased from Aladdin. N-hydroxysuccinimide (NHS) was purchased from Macklin. Phosphate Buffered Saline (PBS) (1×), RPMI-1640 medium, heat inactivated fetal bovine serum (FBS), trypsin EDTA 0.05%, penicillin/

streptomycin (PEST) 10,000 Unit/mL/10,000 mg/mL were purchased from Gibco. Recombinant mouse granulocyte-macrophage colony-stimulating factor (GM-CSF) and interleukin 4 (IL-4) were purchased from R&D. Fluorochrome-labeled anti-mouse monoclonal antibodies (CD11c, CD80 and CD86) were purchased from eBioscience. Anti-mouse ELISA kits interleukin-1β (IL-1β), interleukin-6 (IL-6) and tumor necrosis factor alpha (TNF-α) were purchased from R&D. All other chemicals used in this study were of analytical reagent grade and were used as received.

Characterization

Infrared spectra (4000–400 cm^{-1}) were recorded on Bruker Fourier-transform infrared (FT-IR) in KBr pellets. Thermogravimetric analysis (TGA, NETZSCH, TG209 C) was conducted in air from 30 °C to 850 °C at a rate of 10 °C min^{-1}. The X-ray photoelectron spectroscopy (XPS, UlVAC-PHI, PHI 5000 VersaProbe) measurement was performed to analyze the surface properties quantitatively. Transmission electron microscopy (TEM) was performed on a JEOL-2100 with accelerating voltage of 200 kV. TEM samples were prepared by drop-casting dispersion onto copper grids covered by carbon film. Confocal images were acquired using a Zeiss confocal laser scanning unit mounted on an LSM 710 fixed-stage upright microscope (CLSM). Flow cytometry experiments were performed with a BD FACS Aria II apparatus.

Preparation of Mannose-Modified Multi-Walled Carbon Nanotubes (Man-MWCNTs)

MWCNTs-COOH was prepared by the oxidation of MWCNTs using nitric acid. Briefly, 100 mg MWCNTs was dissolved in 50 mL nitric acid, then stirred at 120 °C for 10 h. The products were collected by centrifugation (8000 rpm, 5 min) and washed with deionized water for three times. In order to synthesis Man-MWCNTs, mannose was first prepared as a mannosylated ethylenediamine according to an established method.[46] After that, MWCNTs-COOH (0.5 mg/mL) was completely dispersed in MES buffer (10 mM, pH 6.0) using an ultrasound bath. EDC (5 mg/mL) and NHS (5 mg/mL) were added and then the mixture was stirred at room temperature for 24 h. The products were collected by centrifugation (10,000 rpm, 5 min) and washed with deionized water for three times. The obtained nanotubes were dispersed in MES buffer and mannosylated ethylenediamine (5 mg/mL) was added, then the mixture was stirred at room temperature for 36 h. The products were collected by centrifugation (11,000 rpm, 5 min) and washed with deionized water for three times.

OVA Loading of Man-MWCNTs (Man-MWCNTs/OVA)

Man-MWCNTs/OVA was obtained after loading ovalbumin protein on the surface of NTs via physical adsorption. Typically, Man-MWCNTs and OVA was dissolved in deionized water with the ratio of 1:1(w/w). The mixture was stirred at room temperature. After 10 h, the mixture was centrifuged at 14,000 rpm for 5 min. The concentration of protein adsorbed on the nanotube was determined by subtracting the concentration of protein remaining in the supernatant (estimated by BCA protein assay) from the total concentration of added protein. Drug loading content (DLC) was calculated according to the following formula: DLC(%) = (weight of loaded OVA/weight of CNTs) × 100%.

The in vitro release behavior of OVA was evaluated using the following method: a 5 mg sample of Man-MWCNTs/OVA aqueous solution was infused into a dialysis bag and dialyzed against phosphate-buffered saline (PBS) with a pH value of 7.4 at 37 °C on an orbital shaker. At each interval time point over a period of 72 h, the concentration of OVA in the dialysate was measured by ultraviolet spectroscopy. The total volume of dialysis was maintained at 50 mL through the test.

Generation of Bone Marrow Derived Dendritic Cells (BMDCs) In Vitro

All animal experiments were performed in compliance with the local ethics committee. Dendritic cells were generated from the bone marrow (BM) of 6- to 8-week-old C57BL/6 mice (18–20 g, Nanjing Mu Tu Medical Science and Technology Co.) according to an established method.[47] Briefly, the femur and tibia were obtained under aseptic conditions and the marrow cells were flushed using RPMI 1640. After treated with red blood cell lysis solution, cells were cultured in six-well plates in complete medium with granulocyte-macrophage colony-stimulating factor (GM-CSF) and interleukin 4 (IL-4) at 2×10^6 cells/4 mL/well. On day 3, the culture medium was replaced by 4 mL fresh medium containing GM-CSF. On day 5, half of the culture medium was harvested and replaced by 2 mL fresh medium containing GM-CSF. On day 7, most of the cells were differentiated into BMDCs and ready for use.

Cell Viability Assay

CCK-8 assay was employed in this experiment to quantitatively evaluate the cell viability. BMDCs were treated with Man-MWCNTs or Man-MWCNTs/OVA with various concentrations for 12 h in 96-well culture plates under the same conditions, respectively. After incubation, 10 μL CCK-8 was added and cultured for another 2 h. The optical density of the solution was measured by enzyme linked immunosorbent assay (ELISA) at a wavelength of 450 nm. The absorbance value of untreated cells was set at 100%. Each experiment was repeated three times in sextuplicate (n = 6).

Confocal Imaging

To detect the intracellular localization of antigen in BMDCs, OVA was pre-labeled with fluorescein isothiocyanate (FITC). Briefly, FITC and OVA was dissolved in 20 mmol/L carbonate buffer (0.5 M, pH 9.5) with the ratio of 1:1(w/w). The solution was incubated with continuous stirring at room temperature for 24 h in the dark. The reaction mixture was dialyzed against distilled water (MWCO 3500) to obtain FITC-OVA.

BMDCs were cultured with FITC-OVA, MWCNTs-COOH/FITC-OVA or Man-MWCNTs/FITC-OVA at 37 °C for 4 h. At the end of the experiment, the cells were labeled with 50 nM Lyso-Tracker Red for 60 min to visualize late endosomes and lysosomes. The nuclei were stained with DAPI for 15 min and fluorescent images were recorded by a confocal laser scanning microscopy.

Flow Cytometry Assay

To detect intracellular OVA signals, FITC-OVA, MWCNTs-COOH/FITC-OVA or Man-MWCNTs/FITC-OVA was incubated with BMDCs for 4 h. After washing the BMDCs with FACS buffer (phosphate buffer saline (PBS) containing 1% FBS), the cellular fluorescence was measured by FCM analysis.

To measure the effects of Man-MWCNTs/OVA on the maturation of BMDCs, BMDCs were also treated with OVA, Man-MWCNTs or Man-MWCNTs/OVA for 12 h. Then cells were washed with FACS buffer and subsequently stained with anti-CD11c-PE–Cy7, anti-CD86-APC, and anti-CD80-PE antibodies (eBioscience) for 30 min at 4 °C. These

BMDCs were then sorted by flow cytometry after being washed again with FACS buffer. All samples were done in triplicate.

Cytokine Detection

BMDCs were cultured with OVA, Man-MWCNTs or Man-MWCNTs/OVA at 37 °C for 24 h. At the end of the experiment, the suspension of BMDCs culture media was diluted for analysis. Interleukin-1β (IL-1β), interleukin-6 (IL-6) and tumor necrosis factor alpha (TNF-α) were analyzed with cytokine-specific ELISA kits respectively according to the vendor's instructions. All samples were measured in triplicate.

Statistical Analysis.

All the data are represented as mean ± standard deviation (SD).

Acknowledgements

The authors gratefully acknowledge the support of the National Natural Sciences Foundation of China (No. 21401216), Innovation Project for Postgraduates in Jiangsu Province (No. KYZZ16_0419), Innovative Training Program for College Students (NO. 201610316029) and Qing Lan Project in Jiangsu Province.

Conflict of Interest

The authors declare no conflict of interest.

Keywords: dendritic cells · carbon nanotubes · antigen presentation · immunotherapy · drug delivery

[1] I. Mellman, G. Coukos, G. Dranoff, *Nature* **2011**, *480*, 480–489.
[2] K. Shao, S. Singha, X. Clemente-Casares, S. Tsai, Y. Yang, P. Santamaria, *ACS Nano* **2015**, *9*, 16–30.
[3] D. N. Khalil, E. L. Smith, R. J. Brentjens, J. D. Wolchok, *Nat. Rev. Clin. Oncol.* **2016**, *13*, 273–290.
[4] L. Gu, D. J. Mooney, *Nat. Rev. Cancer* **2016**, *16*, 56–66.
[5] M. S. Goldberg, *Cell* **2015**, *161*, 201–204.
[6] C. J. Melief, *Immunity* **2008**, *29*, 372–383.
[7] O. Proudfoot, V. Apostolopoulos, G. A. Pietersz, *Mol. Pharm.* **2007**, *4*, 58–72.
[8] F. Aranda, D. Llopiz, N. Diaz-Valdes, J. I. Riezu-Boj, J. Bezunartea, M. Ruiz, M. Martinez, M. Durantez, C. Mansilla, J. Prieto, J. J. Lasarte, F. Borras-Cuesta, P. Sarobe, *Cancer Res.* **2011**, *71*, 3214–3224.
[9] K. T. Gause, A. K. Wheatley, J. Cui, Y. Yan, S. J. Kent, F. Caruso, *ACS Nano* **2017**, *11*, 54–68.
[10] K. Brzezicka, U. Vogel, S. Serna, T. Johannssen, B. Lepenies, N. C. Reichardt, *ACS Chem. Biol.* **2016**, *11*, 2347–2356.
[11] E. J. McKenzie, P. R. Taylor, R. J. Stillion, A. D. Lucas, J. Harris, S. Gordon, L. Martinez-Pomares, *J. Immunol.* **2007**, *178*, 4975–4983.
[12] B. Carrillo-Conde, E. H. Song, A. Chavez-Santoscoy, Y. Phanse, A. E. Ramer-Tait, N. L. Pohl, M. J. Wannemuehler, B. H. Bellaire, B. Narasimhan, *Mol. Pharm.* **2011**, *8*, 1877–1886.
[13] N. Islam, V. Ferro, *Nanoscale* **2016**, *8*, 14341–14358.
[14] K. Raemdonck, K. Braeckmans, J. Demeester, S. C. De Smedt, *Chem. Soc. Rev.* **2014**, *43*, 444–472.
[15] K. Liu, X. Jiang, P. Hunziker, *Nanoscale* **2016**, *8*, 16091–16156.
[16] R. G. Mendes, A. Bachmatiuk, B. Büchner, G. Cuniberti, M. H. Rümmeli, *J. Mater. Chem. B* **2013**, *1*, 401–428.
[17] L. Luo, R. Shu, A. Wu, *J. Mater. Chem. B* **2017**, *5*, 5517–5531.
[18] M. Ahmed, *Biomater. Sci.* **2017**, *5*, 2188–2211.
[19] R. Jijie, A. Barras, R. Boukherroub, S. Szunerits, *J. Mater. Chem. B* **2017**, *5*, 8653–8675.
[20] K. Kostarelos, L. Lacerda, G. Pastorin, W. Wu, S. Wieckowski, J. Luangsivilay, S. Godefroy, D. Pantarotto, J. P. Briand, S. Muller, M. Prato, A. Bianco, *Nat. Nanotechnol.* **2007**, *2*, 108–113.
[21] S. Marchesan, S. Bosi, A. Alshatwi, M. Prato, *Nano Today* **2016**, *11*, 398–401.
[22] S. R. Shin, S. M. Jung, M. Zalabany, K. Kim, P. Zorlutuna, S. B. Kim, M. Nikkhah, M. Khabiry, M. Azize, J. Kong, K. T. Wan, T. Palacios, M. R. Dokmeci, H. Bae, X. W. Tang, *ACS Nano* **2013**, *7*, 2369–2380.
[23] D. Tasis, N. Tagmatarchis, A. Bianco, M. Prato, *Chem. Rev.* **2006**, *106*, 1105–1136.
[24] C. Klumpp, K. Kostarelos, M. Prato, A. Bianco, *BBA-Biomembranes* **2006**, *1758*, 404–412.
[25] J. Xing, Z. Liu, Y. Huang, T. Qin, R. Bo, S. Zheng, L. Luo, Y. Huang, Y. Niu, D. Wang, *ACS Appl. Mater. Interfaces* **2016**, *8*, 19276–19283.
[26] M. Zhu, G. Diao, *Nanoscale* **2011**, *3*, 2748–2767.
[27] M. Adeli, R. Soleyman, Z. Beiranvand, F. Madani, *Chem. Soc. Rev.* **2013**, *42*, 5231–5256.
[28] I. Monaco, S. Camorani, D. Colecchia, E. Locatelli, P. Calandro, A. Oudin, S. Niclou, C. Arra, M. Chiariello, L. Cerchia, M. Comes Franchini, *J. Med. Chem.* **2017**, *60*, 4510–4516.
[29] D. Li, F. Sun, M. Bourajjaj, Y. Chen, E. H. Pieters, J. Chen, J. B. van den Dikkenberg, B. Lou, M. G. Camps, F. Ossendorp, W. E. Hennink, T. Vermonden, C. F. van Nostrum, *Nanoscale* **2016**, *8*, 19592–19604.
[30] S. M. Xue, Z. L. Xu, Y. J. Tang, C. H. Ji, *ACS Appl. Mater. Interfaces.* **2016**, *8*, 19135–19144.
[31] Y. C. Chiang, W. H. Lin, Y. C. Chang, *Appl. Surf. Sci.* **2011**, *257*, 2401–2410.
[32] S. W. Lee, B. S. Kim, S. Chen, Y. Shao-Horn, P. T. Hammond, *J. Am. Chem. Soc.* **2009**, *131*, 671–679.
[33] J. T. Wilson, S. Keller, M. J. Manganiello, C. Cheng, C. C. Lee, C. Opara, A. Convertine, P. S. Stayton, *ACS Nano* **2013**, *7*, 3912–3925.
[34] P. Li, G. Shi, X. Zhang, H. Song, C. Zhang, W. Wang, C. Li, B. Song, C. Wang, D. Kong, *J. Mater. Chem. B* **2016**, *4*, 5608–5620.
[35] S. N. Mueller, S. Tian, J. M. DeSimone, *Mol. Pharm.* **2015**, *12*, 1356–1365.
[36] Z. Sun, V. Nicolosi, D. Rickard, S. D. Bergin, D. Aherne, J. N. Coleman, *J. Phys. Chem. C* **2008**, *112*, 10692–10699.
[37] C. Fabbro, H. Ali-Boucetta, T. Da Ros, K. Kostarelos, A. Bianco, M. Prato, *Chem. Commun.* **2012**, *48*, 3911–3926.
[38] M. Zhang, Y. Hong, W. Chen, C. Wang, *ACS Biomater. Sci. Eng.* **2017**, *3*, 108–125.
[39] Y. Ji, J. Zhao, C. Chu, *J. Mater. Chem. B* **2018**, *6*, 1930–1942.
[40] G. Gunay, M. Sardan Ekiz, X. Ferhati, B. Richichi, C. Nativi, A. B. Tekinay, M. O. Guler, *ACS Appl. Mater. Interfaces* **2017**, *9*, 16035–16042.
[41] X. Liang, X. Li, J. Duan, Y. Chen, X. Wang, L. Pang, D. Kong, B. Song, C. Li, J. Yang, *Mol. Pharm.* **2018**, *15*, 508–518.
[42] D. Krikorian, E. Panou-Pomonis, C. Voitharou, C. Sakarellos, M. Sakarellos-Daitsiotis, *Bioconjugate Chem.* **2005**, *16*, 812–819.
[43] T. H. Kang, N. R. Han, H. M. Kim, H. J. Jeong, *J. Nat. Prod.* **2011**, *74*, 223–227.
[44] R. Ciuffa, E. Caron, A. Leitner, F. Uliana, M. Gstaiger, R. Aebersold, *J. Proteome Res.* **2017**, *16*, 14–33.
[45] X. Zhu, T. Giordano, Q. S. Yu, H. W. Holloway, T. A. Perry, D. K. Lahiri, A. Brossi, N. H. Greig, *J. Med. Chem.* **2003**, *46*, 5222–5229.
[46] M. Sousa, D. S. T. Martinez O. L. Alves, *J. Nanopart. Res.* **2016**, *18*, 143–154.
[47] L. Xu, Y. Liu, Z. Chen, W. Li, Y. Liu, L. Wang, L. Ma, Y. Shao, Y. Zhao, C. Chen, *Adv. Mater.* **2013**, *25*, 5928–5936.

Manuscript received: April 6, 2019
Revised manuscript received: June 17, 2019